# NEDA - NEutron Detector Array

J.J. Valiente-Dobón[a], G. Jaworski[a], A. Goasduff[a,b,c], F.J. Egea[a,b,c,d],

V. Modamio[a,e], T. Hüyük[d], A. Triossi[b,c,f], M. Jastrząb[g], P.A. Söderström[h],

A. Di Nitto[i], G. de Angelis[a], G. de France[j], N. Erduran[k], A. Gadea[d],

M. Moszyński[l], J. Nyberg[m], M. Palacz[n], R. Wadsworth[o], R. Aliaga[d],

C. Aufranc[q], M. Bézard[j], G. Baulieu[q], E. Bissiato[a], A. Boujrad[j], I. Burrows[p],

S. Carturan[a,b], P. Cocconi[a], G. Colucci[b,c], D. Conventi[a], M. Cordwell[p],

S. Coudert[j], J.M. Deltoro[a], L. Ducroux[j], T. Dupasquier[q], S. Ertürk[r],

X. Fabian[q], V. González[s], A. Grant[p], K. Hadyńska-Klęk[a,t], A. Illana[a],

M. L. Jurado-Gomez[d], M. Kogimtzis[p], I. Lazarus[p], L. Legeard[j], J. Ljungvall[u],

G. Pasqualato[b,c], R. M. Pérez-Vidal[d], A. Raggio[a], D. Ralet[j], N. Redon[q],

F. Saillant[j], B. Saygı[v], E. Sanchis[s], M. Scarcioffolo[b,c], M. Siciliano[a],

D. Testov[b,c], O. Stezowski[q], M. Tripon[j], I. Zanon[a]

[a]*Istituto Nazionale di Fisica Nucleare, Laboratori Nazionali di Legnaro, Legnaro, Italy*
[b]*Dipartimento di Fisica e Astronomia, Università di Padova, Padova, Italy*
[c]*Istituto Nazionale di Fisica Nucleare, Sezione di Padova, Università di Padova, Padova, Italy*
[d]*Instituto de Física Corpuscular, CSIC-Universidad de Valencia, E-46980 Paterna (Valencia), Spain*
[e]*Department of Physics, University of Oslo, N-0316 Oslo, Norway*
[f]*CERN, Switzerland*
[g]*Niewodniczanski Institute of Nuclear Physics, Polish Academy of Sciences, Kraków, Poland*
[h]*Extreme Light Infrastructureuclear Physics (ELI-NP), 077125 Bucharest-Magurele, Romania*
[i]*Helmholtz Institute Mainz and GSI Helmholtzzentrum für Schwerionenforschund Darmstadt, Germany*
[j]*GANIL, CEA/DRF-CNRS/IN2P3, Bvd. Henri Becquerel, 14076 Caen, France*
[k]*Faculty of Engineering and Natural Sciences, Istanbul Sabahattin Zaim University, 34303 Istanbul, Turkey*
[l]*National Centre for Nuclear Research, 05-400 Otwock-Świerk, Poland*
[m]*Department of Physics and Astronomy, Uppsala University, SE-75120 Uppsala, Sweden*
[n]*Heavy Ion Laboratory, University of Warsaw, 02-093 Warsaw, Poland*
[o]*Department of Physics, University of York, Heslington, YO10 5DD York, U.K.*
[p]*STFC Daresbury Laboratory, Daresbury, Warrington WA4 4AD, U.K.*
[q]*Université Lyon 1, CNRS, IN2P3, IPN Lyon, F-69622 Villeurbanne, France*
[r]*Department of Physics, University of Nigde, 51240 Nigde, Turkey*
[s]*Departamento de Ingeniería Electrónica, Universidad de Valencia. Avda. Universidad s/n 46100 Burjassot, Spain.*
[t]*Department of Physics, University of Surrey, Guildford GU2 7XH, U.K.*
[u]*CSNSM, CNRS, IN2P3, Université Paris-Sud, F-91405 Orsay, France*
[v]*Department of Physics, Faculty of Science, University of Ege, Izmir, 35100, Turkey*

## Abstract

The NEutron Detector Array, NEDA, will form the next generation neutron detection system that has been designed to be operated in conjunction with $\gamma$-ray arrays, such as the tracking-array AGATA, to aid nuclear spectroscopy studies. NEDA has been designed to be a versatile device, with high-detection efficiency, excellent neutron-$\gamma$ discrimination and high rate capabilities. It will be employed in physics campaigns in order to maximise the scientific output, making use of the different European stable and radioactive ion beams. The

first implemenation of the neutron detector array NEDA with AGATA $1\pi$ was
realized at GANIL. This manuscript reviews the various aspects of NEDA.

## 1. Introduction

The main objective of nuclear structure is to study the nature and phe-
nomenology of the nucleon-nucleon interaction in the nuclear medium. Gamma-
ray spectroscopy represents one of the most powerful methods to study nuclear
structure since a large fraction of the de-excitation of the excited nuclear levels
goes via the emission of $\gamma$ rays. High-resolution $\gamma$-ray spectroscopy makes it pos-
sible to perform high precision measurements that help to determine the energy,
angular momentum and parity of nuclear excited states, as well as transition
probabilities using a variety of techniques. All this information characterizes
the nucleus under study. The knowledge of nuclear matter has progressed *pari
passu* with the technical development of $\gamma$-ray spectrometers and associated an-
cillary devices that the nuclear spectroscopy community has built up over the
last five decades.

The NEutron Detector Array (NEDA) [1, 2, 3, 4, 5, 6, 7, 8] is a neutron
detector array of the next generation. It has been constructed as an ancillary
detector for use with the Advanced Gamma Tracking Array (AGATA), which is
a state-of-the-art high-resolution $\gamma$-ray spectrometer based on the $\gamma$-ray tracking
technique [9]. The first implementation of NEDA has been done with AGATA
$1\pi$ at GANIL [1, 10]. However, other large $\gamma$-ray arrays are also foreseen to
be coupled to NEDA. Neutron and charged-particle detectors provide a good
selection of the decay channels that has been demonstrated to be very efficient
for the study of neutron-deficient nuclei populated by fusion-evaporation re-
actions, e.g. for the investigation of nuclei close to the N=Z line. NEDA is
also a well suited device for the investigation of exotic nuclei populated with
transfer reactions, where the emitted particle is a neutron. A large variety of
new radioactive beams will be accessible in the next years for transfer reactions
induced by proton- and neutron-rich projectiles from radioactive beam facilities
such as HIE-ISOLDE (CERN, Geneva, Switzerland), SPES (Legnaro, Italy),
SPIRAL2 (Caen, France) and FAIR (Darmstadt, Germany). Neutron detectors
based on liquid scintillators that provide neutron-$\gamma$ identification by pulse-shape
discrimination and Time-of-Flight (ToF) have been in use for decades. There
are a few examples of high-efficiency neutron detectors with high discrimination
capabilities between neutrons and $\gamma$ rays that can be coupled to large $\gamma$-ray
arrays, such as Neutron Wall [11, 12], Neutron Shell [13] and DESCANT [14].

The conceptual design of NEDA is discussed in Section 2. The outcome of
our considerations for a broad use of NEDA in different experimental conditions
yielded a design based on a modular array of hexagonal single detectors that can
tile up a compact surface or a hemisphere, see Section 3. Section 4 describes
the fully-digital front-end electronics conceived to obtain excellent neutron-$\gamma$
discrimination capabilities, integration with fully digital modern $\gamma$-ray arrays
and flexibility. Finally, Section 5 discusses the data-acquisition system imple-
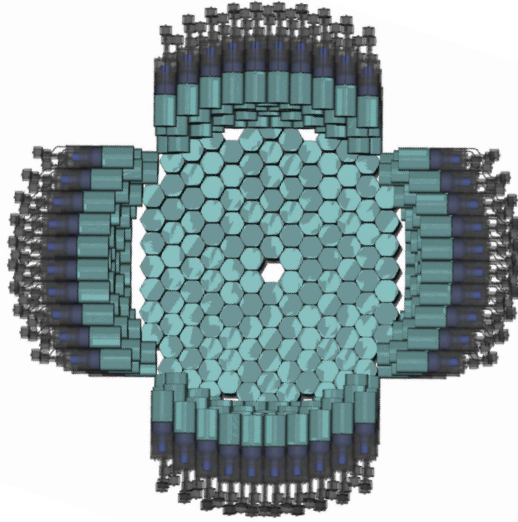mented for NEDA and AGATA.

Figure 1: Proposed NEDA geometry for a $2\pi$ angular coverage at one meter distance. The total number of identical NEDA detectors is 331, covering a solid angle of 1.88 $\pi$ s.r.

## 2. Conceptual design

NEDA is conceptually designed to be a versatile and a highly-efficient neutron detector array with good neutron-$\gamma$ discrimination capabilities at high counting rates. It will be used as a neutron tagging instrument coupled with large $\gamma$-ray arrays at stable and radioactive ion beam facilities, that will efficiently measure neutrons emitted from outgoing channels in fusion-evaporation and low-energy transfer reactions. The kinematics of particles emitted in these two types of nuclear reactions, fusion-evaporation and transfer, demand very different characteristics from a neutron detector. In the former case, the neutrons have a Maxwellian distribution with a maximum at energies of a few MeV and due to the kinematics of the reaction, they have an angular distribution peaked at forward angles with respect to the beam direction. NEDA has specially been optimised to have large efficiency in such fusion-evaporation reactions, for neutron multiplicities 2 and 3. In transfer reactions, the neutrons can reach energies above 10 MeV and their angular distributions highly depend on the angular momentum transferred, energy of the beam, and kinematics of the reaction.

An early implementation of NEDA combined with Neutron Wall and AGATA for fusion-evaporation reactions is described in Ref. [1]. In this first usage of NEDA, a limited number of NEDA detectors were coupled together with the Neutron Wall at approximately half a meter from the target with an angular
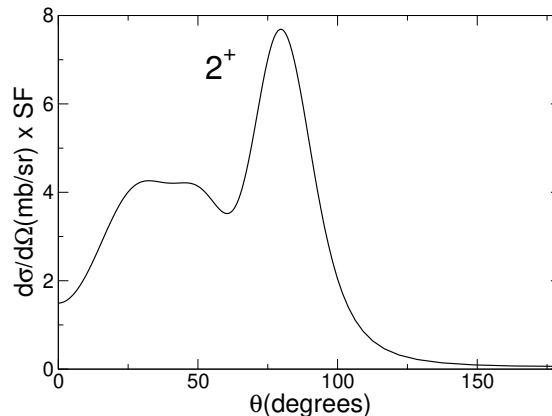
Figure 2: Calculated cross sections for the $2^+$ state with Twofnr [15] as a function of the angle of the emitted neutrons in the laboratory reference frame for the reaction $^3$He($^{18}$Ne,n)$^{20}$Mg at 4.0 MeV×A. SF is the spectroscopic factor, that has been considered one for this case.

coverage of 1.6 $\pi$ s.r. In this reference, a large discussion was dedicated to the validation of the GEANT4 simulations with experimental data. Whereas, the present work is devoted to a discussion of the NEDA $2\pi$ configuration, which will be composed of 331 single NEDA detectors located one meter from the target and covering a solid angle of 1.88 $\pi$ s.r.. The angular coverage for each individual detector is about 7.5°. This configuration will allow for an improvement of not only neutron-$\gamma$ discrimination, based on Time-Of-Flight (TOF) measurements but also the neutron angular resolution, which is essential for measuring, in transfer reactions, the angular momentum transferred. The geometry for the NEDA $2\pi$ configuration at one meter focal distance is shown in Fig. 1. Simulations for this geometry were performed by using the previously developed event generator for GEANT4 simulations, producing neutrons emitted by a $^{252}$Cf source and in the fusion-evaporation reaction $^{58}$Ni + $^{56}$Fe at 220 MeV [1]. In addition, a possible future transfer reaction to be used with NEDA has been considered in the simulations, namely $^3$He($^{18}$Ne,n)$^{20}$Mg at 4.0 MeV×A. For this latter case an isotropic angular distribution as well as a realistic angular distribution for the neutrons, calculated with the DWBA Twofnr code [15], has been used as the event-generator input for the GEANT4 simulations. The flat angular distribution is purely an academic exercise, where the important parameter that will affect the efficiencies is the neutron energy. Figure 2 shows the calculated cross sections for the $2^+$ state as a function of the angle of the emitted neutron in the laboratory reference frame.

Table 1 shows the simulated one-, two- and three-neutron detection efficiencies for emissions from a $^{252}$Cf ($Cf$) source and from the fusion-evaporation reaction $^{58}$Ni + $^{56}$Fe at 220 MeV ($FE$) for a light threshold of 50 keVee. The one-neutron efficiency obtained for the transfer reaction $^3$He($^{18}$Ne,n)$^{20}$Mg at 4.0 MeV per nucleon is also shown. A full angular dependence ($TA$) and a flat distribution ($TF$) have been considered for this physics case. For this study cases ($TA$ and $TF$), the neutrons have an energy of 17 MeV at zero degrees and around 3 MeV at ninety degrees. The simulation that considers the real angular distribution will reflect, in addition to the efficiency for the large energy neutrons, the angular integrated cross-section which is very much dependent

4

Table 1: One-, two- and three-neutron detection efficiencies obtained from simulations of a $^{252}$Cf source ($Cf$) and the fusion-evaporation reaction, $^{58}$Ni (220 MeV) + $^{56}$Fe ($FE$). The one-neutron efficiency, simulated for the transfer reaction $^{3}$He($^{18}$Ne,n)$^{20}$Mg at 4.0 MeV per nucleon, is also shown. For this case a full angular dependence ($TA$) and an isotropic distribution of the emitted neutron ($TF$) have been considered. The final values of the efficiencies have been scaled by the correction factor discussed in Ref. [1]. Results obtained for a light threshold of 50 keVee. Errors quoted are statistical.

| Geometry | $\varepsilon_{1n}$ [%] | $\varepsilon_{2n}$ [%] | $\varepsilon_{3n}$ [%] |
|---|---|---|---|
| NEDA $2\pi$ - Cf | 23.82(15) | 4.33(7) | 0.63(3) |
| NEDA $2\pi$ - FE | 40.54(7) | 11.49(9) | 3.7(2) |
| NEDA $2\pi$ - TA | 42.75(7) | - | - |
| NEDA $2\pi$ - TF | 18.67(4) | - | - |

on each specific beam and target combination, the angular momentum transferred and the energy of the beam. The simulations of the NEDA $2\pi$ version at one meter focal distance can not be directly compared to the results presented in Ref. [1] since in the present simulation a 50 keVee threshold has been utilised, whereas the simulations presented in Ref. [1] were performed with a threshold of 150 keVee for the NEDA detectors and an individual threshold for each Neutron Wall detector. For transfer reactions were high energy neutrons are involved the full NEDA array still keeps a large efficiency as can be seen in Table 1 for the case of a isotropic angular distribution. This is because the NEDA detectors have a significant intrinsic neutron detection efficiency due to their depth of around 20 cm. In addition to the large efficiency of the NEDA $2\pi$ at one meter focal distance, one should consider other aspects: among those aspects it is worth noticing that by exploiting the larger flight path it will be possible to improve the neutron-$\gamma$ discrimination and the energy resolution, due to the longer TOF, as well as the angular resolution, due to the smaller solid angles subtended by each single detector.

## 3. Detectors

The single NEDA detector was carefully designed in order to achieve the best possible efficiency, time resolution, neutron-$\gamma$ discrimination and minimise crosstalk among detectors. Extensive Monte Carlo simulations were carried out to optimise the type of scintillator used, the size of a single detector and its distance to the target and thus the granularity of the array [2]. The final decision was to build individual NEDA detectors with a cross-section fitting a 5 inch Photo Multiplier Tube (PMT) with a length of around 20 cm. The active volume of the detector was filled with the liquid scintillator ELJEN EJ301 (which is equivalent to BC501A). Furthermore, since a highly efficient array was foreseen, a fully tiled up surface was required, with minimum dead layers in between. Only three regular polygons (square, triangle, hexagon) can tile a flat surface without gaps. This can be done by using only one type of these polygons or a combination of several of them. One of the polygons, the regular hexagon, was chosen as the starting point for the NEDA geometry since its profile covers the largest fraction of the area of a photomultiplier with a circular cross section.

A single NEDA detector is shown in Fig. 3. The detector cell is made of 6060 aluminium alloy and has a hexagonal profile with a 146 mm side to side distance, and 3 mm thick walls. It is 205 mm long, with an active volume of
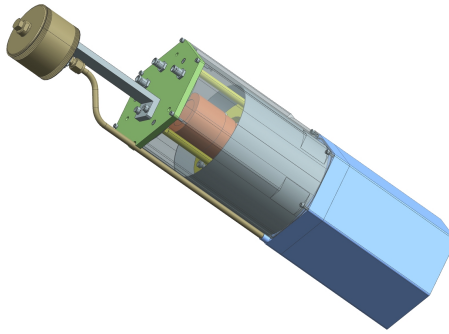
Figure 3: Drawing showing the design of a NEDA neutron detector. It has a hexagonal profile with a cell (blue) where the liquid organic scintillator EJ301 is placed. This cell is connected via a pipe to an expansion bellow (brown). A hexagonal light tight casing contains the Photo Multiplier Tube and voltage divider (orange) as well as a mu-metal shielding (grey). The spring pusher for the PMT is shown in yellow.

$\sim$3.15 litres filled with the liquid organic scintillator EJ301. The inner surface is coated with $TiO_2$-based reflective paint EJ520. The top flange includes a 5 inch N-BK7 5 mm thick glass window, which has 92% transmittance for the wavelength spectrum emitted by the scintillator. A pipe connects the active volume of the detector with an expansion chamber located on the top of the PMT casing. This expansion chamber is needed to allow for the change in volume of the scintillator with temperature. The edge welded bellow (expansion chamber) is 3 inch in diameter and expands up to 153 $cm^3$ in a stroke of 4.8 cm, leading to an operational temperature range of 40 °C with minimal pressure differences. The design of a single NEDA detector has been already described in Ref. [16].

An investigation into the best possible PMT existing in the market that would provide good neutron-$\gamma$ discrimination, as well as the best possible timing, was performed and published in Ref. [3]. From the various PMTs on the market (ET9390-kb produced by ET Enterprises and the Hamamatsu R4144 and R11833-100), it was shown that ET9390-kb and R11833-100 are of similar quality giving a Figure Of Merit (FOM), as defined in Ref. [17] of $\approx$ 1.7 at 320±20 keVee for a commercial test detector, which was significantly better than R4144. Taking into account also the timing properties of the three PMTs, thoroughly discussed in Ref. [4], the final choice was the Hamamatsu PMT of model R11833-100 with a super bialkali photocathode. The voltage divider, designed and constructed within the collaboration for the R11833-100 PMT, is transistorised in order to sustain large counting rates without loosing linearity. Successful linearity tests were performed up to counting rates of $\sim$300 kHz.

The final detector, which is self produced by the NEDA collaboration, has an excellent light yield of 2850±100 photoelectrons per MeVee. The average value is almost a factor of two larger than what was obtained for the previously developed detectors for the EUROBALL Neutron Wall [11]. Figure 4 shows a typical neutron-$\gamma$ discrimination, based on the charge comparison method [17], as a function of light yield in keVee measured with a $^{252}$Cf source. One can note, the excellent separation of the $\gamma$ and neutron distributions even for such large scintillator volume.

6

²¹⁶ Further detailed information on the design, construction, tests and perfor-
²¹⁷ mance of a single NEDA detector will be provided in a forthcoming publica-
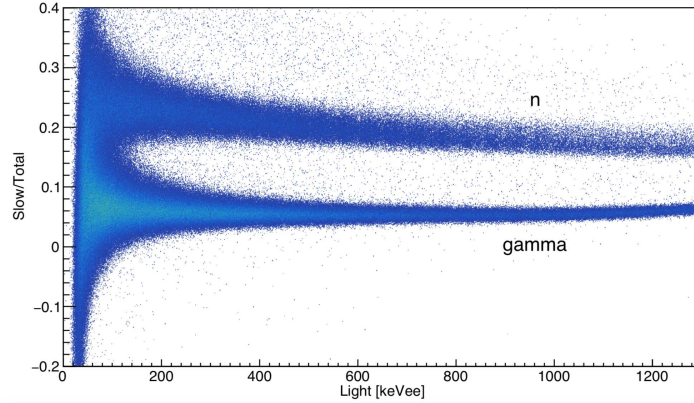²¹⁸ tion [18].



Figure 4: Pulse-shape discrimination based on the charge comparison method [17] measured
with a NEDA detector using a $^{252}$Cf source. The ratio of the light in the slow component of
the digitised signal divided by the total light is shown on the y axis as a function of the total
light in keVee on the x axis.

## 4. Front-end electronics

²²⁰ NEDA Front-End Electronics (FEE), unlike its predecessor the Neutron
²²¹ Wall, is fully-digital and envisaged to improve the neutron-$\gamma$ discrimination,
²²² as well as the processing capabilities, integration and overall flexibility [5]. As
²²³ mentioned before, NEDA is primarily designed to be used together with various
²²⁴ Ge detector systems, in particular with AGATA, EXOGAM2 [19, 20] and the
²²⁵ GALILEO [21] arrays. In order to facilitate this coupling, the electronics of
²²⁶ NEDA uses the Global Trigger and Synchronisation (GTS) system [22].

²²⁷ The detector photomultiplier tube delivers a current signal through a 15-
²²⁸ m-long shielded coaxial cable to a NIM module that provides the Single-Ended
²²⁹ to DIFFerential (SE-DIFF) conversion. SE-DIFF delivers differential analog
²³⁰ signals to the digitizers and pre-processing modules by means of HDMI ca-
²³¹ bles. These two sets of cables have been selected carefully to cope with the sig-
²³² nal bandwidth and crosstalk performance requirements of NEDA. The shielded
²³³ coaxial 15-m cables have a -0.43 dB @ 480 MHz. While the 1.5-m HDMI cables
²³⁴ have a bandwidth of 430 MHz and crosstalk levels of -42.29/-48.11 dB for signals
²³⁵ with rise-times of 3 and 7 ns, respectively.

²³⁶ The SE-DIFF module has been developed in the NIM standard and contains
²³⁷ a PCB board capable of converting the signals of 16 detectors. The board uses
²³⁸ a fully-differential amplifier AD8139 and each channel is adapted to work in a
²³⁹ range of 3 V, although the input range can be increased up to 8 V, activating a
²⁴⁰ voltage divider available at the input stage.

²⁴¹ The core of the FEE is the NUMEXO-2 cards developed for EXOGAM2,
²⁴² which consist of a set of 4 Flash Analog-to-Digital-Converter (FADC) Mezza-
²⁴³ nines in charge of digitising the signals at 200 Msps. The FADC mezzanines

7

contain each four Analog-to-Digital (A/D) modules. In addition, the cards contain a motherboard which includes two large FPGAs used to perform the trigger generation, digital signal processing, clocking, data packaging and readout tasks to the servers for 16 independent channels.

The FADC Mezzanine is the daughterboard in charge of the A/D conversion, whose sampling frequency and resolution specifications have been selected on the basis of the signal properties to be digitised [6, 7]. These specifications do not come only from the NEDA project since the FADC Mezzanines were also designed for other projects such as EXOGAM2. The major resolution constraint comes from the EXOGAM side whose specification of 2.3 keV @ 1.33 MeV led to a choice of an ADC with ENOB > 11.3. To fulfil the various needs of NEDA and EXOGAM2 the final choice was to use the ADS62P49 sampling device, providing a board with 4 channels sampling at 200 Msps with an ENOB of 11.6-11.7 bits. As for the clock, the main 100 MHz clock from the GTS is obtained, and processed with a jitter cleaner in order to produce a 200 MHz sampling clock. At the input of the FADC Mezzanine, an analog fully-differential coupling stage adapts the input range to the ADC chip range, with the added capability of a controllable offset which permits use of the full FADC dynamics.

The NUMEXO-2 motherboard includes two FPGAs, a Virtex-6 and a Virtex-5, which carry out the pre-processing tasks. The Virtex-6 FPGA performs the data processing, trigger elaboration, package building and formatting, whereas the Virtex-5 FPGA manages the readout via PCIe, slow control via Ethernet, integration of the GTS leaf and implementation of the ADC interface, which is the block in charge of storing temporarily the data before validation by the GTS system. A descriptive view of how the blocks are structured inside the FPGA is depicted in Fig. 5. In the following paragraphs the functionalities included in the two NUMEXO-2 FPGAs will be discussed.
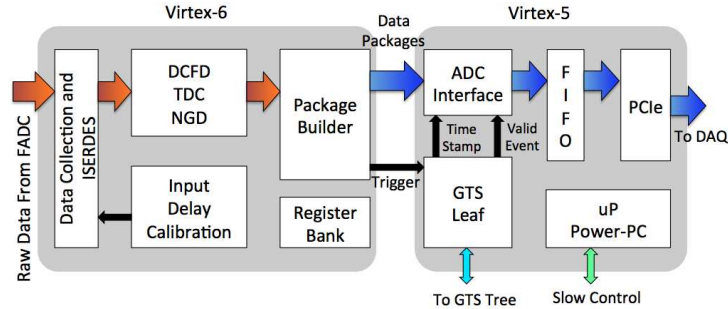


Figure 5: Block diagram depicting the main blocks in the NUMEXO-2 as well as the interaction among them.

The first block found at the beginning of the Virtex-6 is a customized arrangement of serialization/deserialization sub-blocks (called ISERDES), used to convert the multiplexed bit pairs provided from the FADCs into processable samples. After that, the first component that the data finds is a baseline cancellation block and a first-level local trigger based either on a leading edge or a Digital Constant Fraction Discriminator (DCFD). The first-level trigger enables a Pulse Shape Analysis (PSA) for neutron-$\gamma$ discrimination based on

the charge-comparison method [17], that will provide the Trigger Request used in the GTS Validation/Rejection cycle [22]. Note that, for this block, parameters such as the fast and slow signal component integration times, as well as the discrimination threshold, are programmable. In parallel, a Time-of-Flight evaluation is done with a TDC process in the FPGA, calculating the time between the DCFD zero-crossover signal and an external reference signal, which is normally provided by the accelerator. The Trigger Request could be also generated by a time condition on the TDC result and can be combined with the PSA Trigger Request with boolean AND or OR conditions. Eight LVDS data lanes communicating with both FPGAs at rates up to 400 MB/s allow a sustained counting rate of 20 kHz trigger request in the 16 channels present in the NUMEXO-2 board. The data frames created in the Virtex-6 FPGA are compatible with the MFM GANIL data format specification. As mentioned in the previous sub-section, the GTS standard has been chosen for NEDA. A specific implementation of the GTS leaf, supporting the 16 Trigger Request of a NEDA NUMEXO-2 board, has been implemented in the Virtex-5 FPGA. The ADC interface process stores temporarily the data buffers and waits for the GTS validation prior to sending the evaluated and sample data information via the PCIe interface. NEDA uses the NUMEXO-2 4x PCIe v1.0 Endpoint link to read out the data. The data are sent to a server (one server per NUMEXO-2) via an MPO optical fibre. On the receiver side, a commercial PCIe bridge card is hosted in the server and converts the optical input to the PCIe legacy bus standard. The Virtex-5 FPGA includes a PowerPC (PPC) 440 processor, running an embedded Linux OS, that manages the slow control and GTS services.

## 5. Data acquisition

In its first implementation at GANIL, the array was used together with AGATA, DIAMANT [23] and the Neutron Wall. In this setup, a total of 54 NEDA detectors and 42 Neutron Wall detectors were used. The signals from the 96 neutron detectors were digitised by six NUMEXO-2 cards. In order to ensure compatibility of the data acquisition systems of NEDA and AGATA, the choice was made to base the data acquisition on the NARVAL system. This system, developed by IPN Orsay, uses the ADA language to manage the data flux through several steps from the producer receiving the data from the electronics down to the event reconstruction and merging of NEDA data together with the AGATA and DIAMANT data. The architecture of the acquisition system for one NUMEXO-2 board is presented in Fig. 6. The transmission of the data between the different actors is integrated in the NARVAL system and based on the TCP/IP and InfiniBand protocols for actors located on separated servers, or UNIX FIFO for actors on the same server. Thanks to the flexibility of the NARVAL system C++ actors developed, within the AGATA-NEDA collaboration, are in charge of the data treatment and can be integrated through shared libraries loaded in the NARVAL environment.

In Section 4, it was shown that the slow-control and the alignment of the GTS system is controlled through the ethernet. To ensure the time alignment of the GTS of NEDA and AGATA, the NUMEXO-2 boards are inserted in a sub-network of the AGATA electronics network. The data transfer of the raw events corresponding to a header containing the channel identification and timing information is made through a dedicated optical link. Thus, each of the 6

NUMEXO-2 boards necessary to accommodate the 96 channels of the NEDA-NeutronWall array, plus one spare board, are optically connected to dedicated servers in charge of the data pre-processing. Commercial PCI-express optical bridges from Samtec are used to make the link between the NUMEXO-2 digitizers and the servers. After this optical transmission, the processed data transit through two different networks: the GANIL network, where all the local processing of the data and the storage of the raw events is done and the AGATA network, on which the two data (NEDA and AGATA) sets are combined. A schematic view of the data acquisition system is shown in Fig. 6.
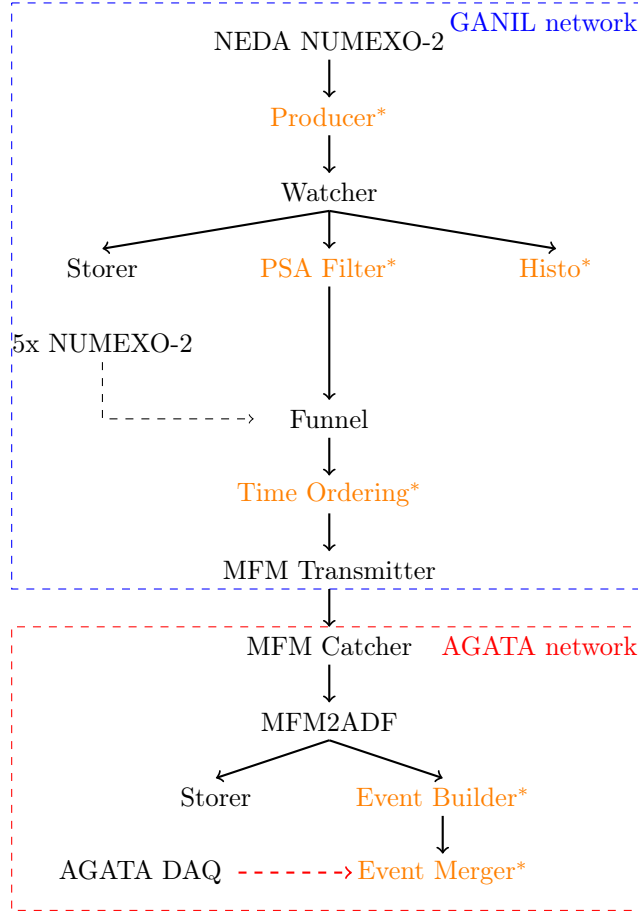


Figure 6: Schematic view of the NEDA data acquisition system. The actors marked with an asterisk are actors developed in C++ within the collaboration. The other actors are standard NARVAL actors. The NEDA acquisition system is shared between two networks: the GANIL and the AGATA network. The transmission of the data between the two networks is performed by one bridge.

A dedicated C++ actor, called Producer in Fig. 6, has been developed to extract the events from the Direct Memory Access (DMA) and transmit them into the NARVAL environment. The data are then transmitted to a standard actor which is in charge of copying the data to three different branches and sending them to three actors: i) a storer, which is used to remotely store the

10

full events with the captured traces (digitised signals) on disk that allows for reprocessing the events offline with advanced PSA algorithms such as a Neural Network (NN) [24, 25], ii) a histogrammer, indicated by Histo in Fig. 6, for data quality monitoring, and, finally, iii) an online PSA code.

Three different algorithms have been implemented in the PSA Filter: a Charge-Comparison (CC) algorithm, similar to the one used at the FPGA level, an integrated rise-time algorithm and finally the Neural Network algorithm described in Ref. [25]. In order to limit the quantity of data transmitted on the network, the choice was made to discard the traces at the output of the PSA filter. The reduced frame, containing only the parameters out of the pulse shape algorithms and the frame header are transmitted though Ethernet to a server, where a NARVAL actor concatenates the data from the 6 servers into a single output transmitted to a time ordering filter. This stage of time ordering is essential as the Funnel in Fig. 6 only loops over the 6 inputs and passes the input buffers in the order of the input branches. It is also for this reason, that the detectors are distributed over the different boards in a pie like configuration in order to distribute the counting rate on each of them as equally as possible. It is only after the time sorting that the data are transmitted frame-by-frame to the AGATA acquisition system, in a manner similar to that used for the VAMOS++ campaign [10], namely by using the MFMTransmitter and MFMCatcher actors. Once in the AGATA world, the MFM frames are encapsulated into AGATA Data Format (ADF) frames using a dedicated key. In order to make the replay of the data faster, a storer is implemented at the output of this actor. Indeed, this allows offline building of the NEDA events directly in the AGATA world without having to do a full PSA analysis of the traces. Before merging the NEDA and AGATA data together, the NEDA events are reconstructed in order to extract the real neutron multiplicity using neutron scattering algorithms.

## 6. Summary

The NEutron Detector Array, NEDA, has been designed to be a versatile device, with high detection efficiency, excellent neutron-$\gamma$ discrimination and high count rate capabilities. NEDA will be used together with large $\gamma$-ray arrays at stable and radioactive beam facilities such as HIE-ISOLDE (CERN, Geneva, Switzerland), LNL/SPES (Legnaro, Italy), GANIL/SPIRAL2 (Caen, France) and FAIR (Darmstadt, Germany). The physics challenges that NEDA will be facing in the near future will be the study of neutron-deficient nuclei populated with fusion-evaporation reactions, close to N=Z as well as transfer studies where the emitted particles are neutrons. NEDA will be comprised of 331 detectors, filled with EJ301 liquid scintillator, where each single detector has an hexagonal profile that allows for a fully tiled up surface. The detector cross-section fits a 5 inch Photo Multiplier Tube (PMT) and it has a length of around 20 cm. A photomultiplier with a super bialkali photocathode (R11833-100) and a transistorised voltage divider to sustain large counting rates are used for the read out. The detectors, which are self-made by the NEDA collaboration, have excellent neutron-$\gamma$ discrimination and timing properties. The NEDA front-end electronics is fully digital and uses the Global Trigger and Synchronisation system to improve processing capabilities, flexibility and integration with other detector systems, in particular $\gamma$-ray arrays such as AGATA. The core of the front-end electronics are the NUMEXO-2 cards that consist of a set of four

11

FADC Mezzanines, each containing four 200 Msps digitisers. The motherboards of the cards contain two FPGA units, a Virtex-6 and a Virtex-5, which carry out the pre-processing tasks. The data acquisition system of NEDA in its first implementation with AGATA is based on the NARVAL system.

## 7. Acknowledgements

## References

[1] T. Hüyük, A. Di Nitto, G. Jaworski, A. Gadea, J. J. Valiente-Dobón, J. Nyberg, M. Palacz, P.-A. Söderström, R. J. Aliaga-Varea, G. de Angelis, et al., Conceptual design of the early implementation of the neutron detector array (neda) with agata, The European Physical Journal A 52 (3) (2016) 1–8.

[2] G. Jaworski, M. Palacz, J. Nyberg, G. De Angelis, G. De France, A. Di Nitto, J. Egea, M. Erduran, S. Ertürk, E. Farnea, et al., Monte carlo simulation of a single detector unit for the neutron detector array neda, Nuclear Instruments and Methods in Physics Research Section A: Accelerators, Spectrometers, Detectors and Associated Equipment 673 (2012) 64–72.

[3] X. Luo, V. Modamio, J. Nyberg, J. Valiente-Dobón, Q. Nishada, G. De Angelis, J. Agramunt, F. Egea, M. Erduran, S. Ertürk, et al., Test of digital neutron–gamma discrimination with four different photomultiplier tubes for the neutron detector array (neda), Nuclear Instruments and Methods in Physics Research Section A: Accelerators, Spectrometers, Detectors and Associated Equipment 767 (2014) 83–91.

[4] V. Modamio, J. Valiente-Dobón, G. Jaworski, T. Hüyük, A. Triossi, J. Egea, A. Di Nitto, P.-A. Söderström, J. A. Ros, G. De Angelis, et al., Digital pulse-timing technique for the neutron detector array neda, Nuclear Instruments and Methods in Physics Research Section A: Accelerators, Spectrometers, Detectors and Associated Equipment 775 (2015) 71–76.

[5] F. E. Canet, V. González, M. Tripon, M. Jastrzab, A. Triossi, A. Gadea, G. De France, J. Valiente-Dobón, D. Barrientos, E. Sanchis, et al., Digital front-end electronics for the neutron detector neda, IEEE Transactions on Nuclear Science 62 (3) (2015) 1063–1069.

12

[6] F. E. Canet, V. González, M. Tripon, M. Jastrzab, A. Triossi, A. Gadea, G. De France, J. Valiente-Dobón, D. Barrientos, E. Sanchis, et al., A new front-end high-resolution sampling board for the new-generation electronics of exogam2 and neda detectors, IEEE Transactions on Nuclear Science 62 (3) (2015) 1056–1062.

[7] F. J. Egea, E. Sanchis, V. González, A. Gadea, J. M. Blasco, D. Barrientos, J. V. Dobón, M. Tripon, A. Boujrad, C. Houarner, et al., Design and test of a high-speed flash adc mezzanine card for high-resolution and timing performance in nuclear structure experiments, IEEE Transactions on Nuclear Science 60 (5) (2013) 3526–3531.

[8] X. L. Luo, V. Modamio, J. Nyberg, J. J. Valiente-Dobon, Q. Nishada, G. De Angelis, J. Agramunt, F. J. Egea, M. N. Erduran, S. Erturk, G. De France, A. Gadea, V. González, A. Goasduff, T. Hüyük, G. Jaworski, M. Moszyński, A. Di Nitto, M. Palacz, P.-A. Söderström, E. Sanchis, A. Triossi, R. Wadsworth, Pulse pile-up identification and reconstruction for liquid scintillator based neutron detectors, Nuclear Inst. and Methods in Physics Research, A 897 (2018) 59–65.

[9] S. Akkoyun, A. Algora, B. Alikhani, F. Ameil, G. De Angelis, L. Arnold, A. Astier, A. Atac, Y. Aubert, C. Aufranc, et al., Agata: advanced gamma tracking array, Nuclear Instruments and Methods in Physics Research Section A: Accelerators, Spectrometers, Detectors and Associated Equipment 668 (2012) 26–58.

[10] E. Clément, C. Michelagnoli, G. de France, H. Li, A. Lemasson, C. B. Dejean, M. Beuzard, P. Bougault, J. Cacitti, J.-L. Foucher, et al., Conceptual design of the agata 1π array at ganil, Nuclear Instruments and Methods in Physics Research Section A: Accelerators, Spectrometers, Detectors and Associated Equipment 855 (2017) 1–12.

[11] Ö. Skeppstedt, H. Roth, L. Lindström, R. Wadsworth, I. Hibbert, N. Kelsall, D. Jenkins, H. Grawe, M. Górska, M. Moszyński, et al., The euroball neutron wall–design and performance tests of neutron detectors, Nuclear Instruments and Methods in Physics Research Section A: Accelerators, Spectrometers, Detectors and Associated Equipment 421 (3) (1999) 531–541.

[12] J. Ljungvall, M. Palacz, J. Nyberg, Monte carlo simulations of the neutron wall detector system, Nuclear Instruments and Methods in Physics Research Section A: Accelerators, Spectrometers, Detectors and Associated Equipment 528 (3) (2004) 741–762.

[13] D. Sarantites, W. Reviol, C. Chiara, R. Charity, L. Sobotka, M. Devlin, M. Furlotti, O. Pechenaya, J. Elson, P. Hausladen, et al., Neutron shell: a high efficiency array of neutron detectors for $\gamma$-ray spectroscopic studies with gammasphere, Nuclear Instruments and Methods in Physics Research Section A: Accelerators, Spectrometers, Detectors and Associated Equipment 530 (3) (2004) 473–492.

[14] P. E. Garrett, DESCANT – the deuterated scintillator array for neutron tagging, Hyperfine Interactions 225 (1-3) (2013) 137–141.

13

[15] M. Igarashi, J. Tostevin, Computer Program TWOFNR (Surrey University version), private communication.

[16] V. Modamio, et al., First Prototype of the NEDA detector array, INFN-LNL Annual Report (241).

[17] P.-A. Söderström, J. Nyberg, R. Wolters, Digital pulse-shape discrimination of fast neutrons and rays, Nuclear Instruments and Methods in Physics Research Section A: Accelerators, Spectrometers, Detectors and Associated Equipment 594 (1) (2008) 79–89.

[18] G. Jaworski, et al.

[19] G. De France, EXOGAM: A $\gamma$-ray spectrometer for exotic beams, in: Exotic nuclei and atomic masses (ENAM 98). AIP Conference Proceedings, GANIL, BP 5027, 14076 Coen Cedex 5, France, 1998, pp. 977–980.

[20] S. L. Shepherd, P. J. Nolan, D. M. Cullen, D. Appelbe, J. Simpson, J. Gerl, M. Kaspar, A. Kleinboehl, I. Peter, M. Rejmund, H. Schaffner, C. Schlegel, G. De France, Measurements on a prototype segmented Clover detector, Nuclear Instruments and Methods in Physics Research Section A 434 (2) (1999) 373–386.

[21] J. Valiente-Dobón, et al., Status of the Gamma-Ray Spectrometer GALILEO, INFN-LNL Annual Report (95).

[22] M. Bellato, D. Bortolato, J. Chavas, R. Isocrate, G. Rampazzo, A. Triossi, D. Bazzacco, D. Mengoni, F. Recchia, Sub-nanosecond clock synchronization and trigger management in the nuclear physics experiment AGATA, Journal Of Instrumentation 8 (07) (2013) P07003–P07003.

[23] J.-N. Scheurer, M. Aiche, M. M. Aléonard, G. Barreau, F. Bourgine, D. Boivin, D. Cabaussel, J. F. Chemin, T. P. Doan, J. P. Goudour, M. Harston, A. Brondi, G. La Rana, R. Moro, E. Vardaci, D. Curien, Improvements in the in-beam $\gamma$-ray spectroscopy provided by an ancillary detector coupled to a Ge $\gamma$-spectrometer: the DIAMANT-EUROGAM II example, Nuclear Instruments and Methods in Physics Research Section A: Accelerators, Spectrometers, Detectors and Associated Equipment 385 (3) (1997) 501–510.

[24] E. Ronchi, P.-A. Söderström, J. Nyberg, E. A. Sundén, S. Conroy, G. Ericsson, C. Hellesen, M. G. Johnson, M. Weiszflog, An artificial neural network based neutron–gamma discrimination and pile-up rejection framework for the BC-501 liquid scintillation detector, Nuclear Instruments and Methods in Physics Research Section A: Accelerators, Spectrometers, Detectors and Associated Equipment 610 (2) (2009) 534–539.

[25] P.-A. Söderström, et al., Neutron detection and $\gamma$-ray rejection using artificial neural networks with the liquid scintillators BC-501A and BC-537, Nuclear Instruments and Methods in Physics Research Section A: Accelerators, Spectrometers, Detectors and Associated Equipment to be submitted.